International Journal of Nanoscience and Nanoengineering
2018; 4(4): 66-73
http://www.openscienceonline.com/journal/nano

High Performance Nitrogen-Doped Disordered Carbon Derived from Cirsium Setosum Anode for Sodium Ion Batteries

Qinggang Wang[1, 2], Jianfeng Huang[1, *], Caiwei Wang[1], Zhanwei Xu[1], Jiayin Li[1, 2], Yijun Liu[2, *]

[1]School of Materials Science & Engineering, Shaanxi University of Science and Technology, Xi'an, China

[2]Monalisa Group Co., Ltd, Foshan, China

Email address

17156587@qq.com (Qinggang Wang), huangjfsust@126.com (Jianfeng Huang)

[*]Corresponding author

To cite this article

Qinggang Wang, Jianfeng Huang, Caiwei Wang, Zhanwei Xu, Jiayin Li, Yijun Liu. High Performance Nitrogen-Doped Disordered Carbon Derived from Cirsium Setosum Anode for Sodium Ion Batteries. *International Journal of Nanoscience and Nanoengineering.* Vol. 4, No. 4, 2018, pp. 66-73.

Received: July 22, 2018; **Accepted**: August 14, 2018; **Published**: September 13, 2018

Abstract

Nitrogen-doped carbon (HNC) derived from cirsium setosum are prepared by hydrothermal carbonization with subsequant heat treatment. The obtained carbon structure was carefully characterized by X-ray diffraction, Scanning electron microscopy, Transmission electron microscopy, raman spectrum and X-ray photoelectron spectrum. The results present a rough lamellar morphology with high lattice spacing of the (002) plane in graphite structure. It is also found nitrogen was successfully doped into the disordered carbon. When employed as anodes for sodium ion batteries (SIBs), electrochemical results show that the HNC treated at 700°C exhibit a high maximum charge capacity of 296.3 mA h g^{-1} at a current density of 50 mA g^{-1}. Even at a high current density of 500 m A g^{-1}, a capacity of 204.7 mA h g^{-1} is maintained after 200 cycles without obvious decay. This performance is much higher than the carbon material obtain without nitrogen doping. Further research reveal the HNC sample could maintain high charge conductivity with low electron transfer resistance even after many cycles of the battery. Therefore, it is believed the doped nitrogen in our disordered carbon could not only provide many extra sodium storage sites, but also enhanced electrochemical kinetic for the charge/discharge process of Na^+. Finally, the high capacity, excellent rate performance, long life cycling and ultrafast rechargeable ability enable the NC to be a promising candidate for practical SIBs.

Keywords

Nitrogen-Doped Carbon, Cirsium Setosum, Sodium Ion Batteries, Low-Cost Anodes

1. Introduction

Increasing demands for energy have become a growing global concern and stimulated extensive interests in more efficient energy storage systems in the form of batteries [1, 3]. In the last decades, lithium ion batteries (LIBs) have been developed successfully as a power source for portable electronics owing to their outstanding energy and power density since their first commercialization in 1991 [4, 8]. However, concerns of large scale deployment of LIBs arise due to the limitation of terrestrial lithium reserves, which triggers increasing attentions to develop new rechargeable battery systems [9, 13]. Sodium is the second alkali metal next to lithium and they have similar chemical properties. Because sodium is distributed in the ocean at almost unlimited levels, sodium ion batteries (SIBs) have recently attracted many attentions as a low cost alternative to LIBs for large-scale energy storage applications [14, 15]. However, the radius of sodium ions (1.02 Å) is much larger than that of lithium ions (0.76 Å), which means that it is difficult to find suitable host materials with sufficiently large interstitial spaces for sodium ion insertion [16, 18]. As a result, exploring suitable electrode materials is crucial for the development of SIBs.

For anode materials, graphite, the most practical choice for LIBs, exhibits an extremely low capacity for SIBs, due to the mismatch between the interlayer distance inside graphite and the size of sodium ions [19, 25]. Disordered carbon appears to

be more suitable anode material for SIBs, due to its large interlayer distance and disordered structure [26]. Previous pioneering works have demonstrated reversible sodium ion intercalation in a variety of carbonaceous materials, such as petroleum cokes, carbon black, intercalation was carried out at extremely low current density within a limited number of cycles in most of those works, the feasibility of using disordered carbon for SIBs was proved. Recently, remarkable progress has been made, revealing that further-developed disordered carbon with improved capacity and cycle stability is promising for practical SIBs. It is reported that carbon microspheres prepared from resorcinol formaldehyde achieved an initial reversible capacity of 285 mAh g^{-1} at a current density of 40 mA cm^{-2} [27]. Komaba et al. discovered a hard carbon material that could deliver a reversible capacity of 240 mA h g^{-1} at a current density of 25 mA g^{-1} and maintain 200 mAh g^{-1} over 100 cycles [28]. Cao's group found that hollow carbon nanowires, prepared from a pyrolyzed hollow polyaniline nanowire precursor, displayed a high reversible capacity of 251 mAh g^{-1} at 50 mA g^{-1} and good cycling stability after 400 cycles [29]. Despite these progresses to date, good cycling stability during long-term cycling, in particular at high current density, which is critical for practical SIBs [30, 31].

Currently an effective strategy to enhance the performance of carbon electrodes for SIBs is nitrogen (N) doping [32-35]. Different kinds of N-doped carbon materials, such as N-doped carbon nanofibers [32, 33], nanosheets [34] and nanofoams [35] have shown much improved electrochemical performance as compared with their un-doped counterparts for SIBs. A green route to synthesize low-cost and high-performance cirsium setosum, of the most abundant biomass resources on earth, which composes of simple reducing sugars, cellulose, hemi-celluloses, lignin and associated phenolic acids. In this work, N-doped carbon (HNC) derived from cirsium setosum was prepared through hydrothermal pretreatment and thermal treatment and they exhibit high capacity, excellent rate capability, especially superior long life cycling stability and ultrafast rechargeable ability.

2. Experimental

2.1. Synthesis

The precursor of cirsium setosum grown in the campus of Shaanxi University of Science and Technology (Shaanxi, China). Before carbonizations, the precursor leaves were thoroughly cleaned using deionized water and EtOH, dried by freeze and cut into small piece. For carbonizing the precursor through hydrothermal process followed high temperature pyrolysis, typically, 3 g precursor and 50 mL of diluted sulfuric acid were placed in a 100 mL stainless steel autoclave and heated at 180°C for 24 h firstly. After being cooled to room temperature naturally, the solid product was collected by filtration, washed with distilled water, and dried. The melamine and the solid product, in a mass ratio of 0:1 or 2:1, were thoroughly ground in an agate mortar, and then the mixture was heated at 700°C with a heating rate of 5°C min^{-1} for 2 h under vacuum condition in a tubular furnace. After that, the activated samples were thoroughly washed with 2 M HCl and distilled water, and dried. The obtained carbons were denoted as HC and HNC.

2.2. Characterization

The obtained of carbons were characterized by X-ray diffraction (XRD, D/max2200PC, Rigaku, Japan) and Raman spectroscopy (RAMAN, Renishaw-invia, Britain). The morphology of carbons were observed by scanning electron microscope (SEM, S-4800, Hitachi, Japan) and X-ray photo-electron spectroscopy (XPS) measurements were performed on an Imaging Photoelectron Spectrometer (Axis Ultra, Kratos Analytical Ltd) with a mono-chromatic Al K a X-ray source. The specific surface area, pore volume and mean pore diameter were evaluated with an ASAP 2020 Accelerated Surface Area and Porosimetry System (Norcross, GA) based on the Brunauer-Emmett-Teller multipoint (BET) method.

2.3. Electrochemical Measurement

Electrochemical measurements were performed using CR2032 coin- type cells. The working electrodes were fabricated by spreading the mixed slurry of the active materials, acetylene black and polyvinylidene fluoride binder in a solvent of N-methyl-2-pyrrolidone with a weight ratio of 80:10:10 onto copper foil, and then drying at 80°C in a vacuum for 12 h. The typical loading amount of active material was 2 - 2.5 mg cm^{-2}. Sodium pellet was used as a counter electrode. The electrolyte was a solution of 1 M $NaClO_4$ in a mixture of ethylene carbonate and diethyl carbonate (EC:DEC=1:1). The cells were charged and discharged using a Neware battery tester (Neware, Shenzhen) with a potential range of 0.01–3.00 V. Cyclic voltammetry (CV) measurements spectroscopy was performed by a CHI660E electrochemical station (Shanghai Chenhua, China). Electrochemical impedance spectroscopy (EIS) measurement was carried out on the same electrochemical workstation in a frequency range of 0.01 Hz to 100 kHz. All tests were performed at 20°C.

3. Results and Discussion

The as-prepared HNC and HC were firstly examined by XRD. The patterns are shown in the Figure 1a. Both HNC and HC show only one broad peak around 24° corresponded to the (002) diffraction modes of the graphitic structure. The graphitic interlayer distance of HNC and HC calculated from Bragg's law for d (002) were about 0.386 and 0.382 nm, which are larger than that of graphite at 0.34 nm. In addition, the low intensity of these peaks suggested that the low degree of crystallinity and the existence of disorder structure [36, 41]. The disorder structure of HNC and HC could be further confirmed by Raman spectroscopy. The Raman spectra of

HNC and HC shown in Figure 1b, there are two broad peaks at 1321 and 1582 cm^{-1} corresponding to the disordered (D) band and graphite (G) band. Generally, the intensity ratio of D band to G band (I_D /I_G) is used to estimate the disorder degree of carbon material. As show in Figure 1b, the I_D /I_G of HNC and HC are 1.12 and 1.04, respectively, which are higher than that of graphene (0.86). This result indicates high disorder structure of HNC and HC [42]. For the storage of sodium ion, the disorder structure usually shows more active sites and higher capacity than that of graphite.

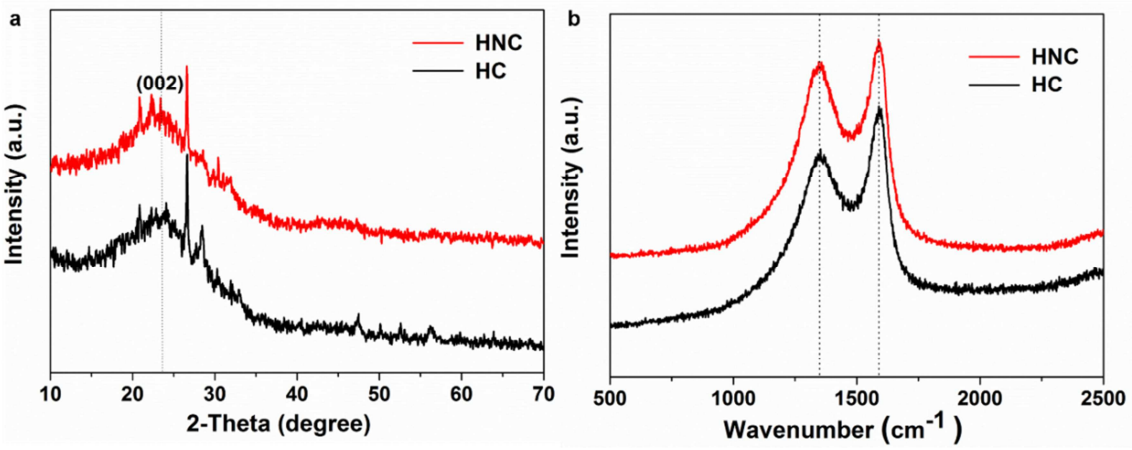

Figure 1. *(a) XRD patterns and (b) Raman spectra of HNC and HC.*

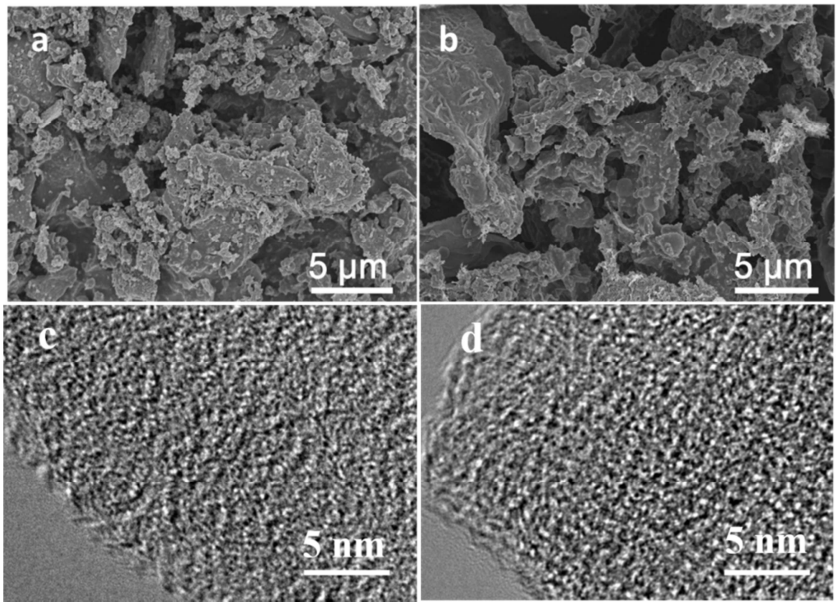

Figure 2. *(a) SEM and (c) HRTEM images of HNC; and (b) SEM and (d) HRTEM images of HC.*

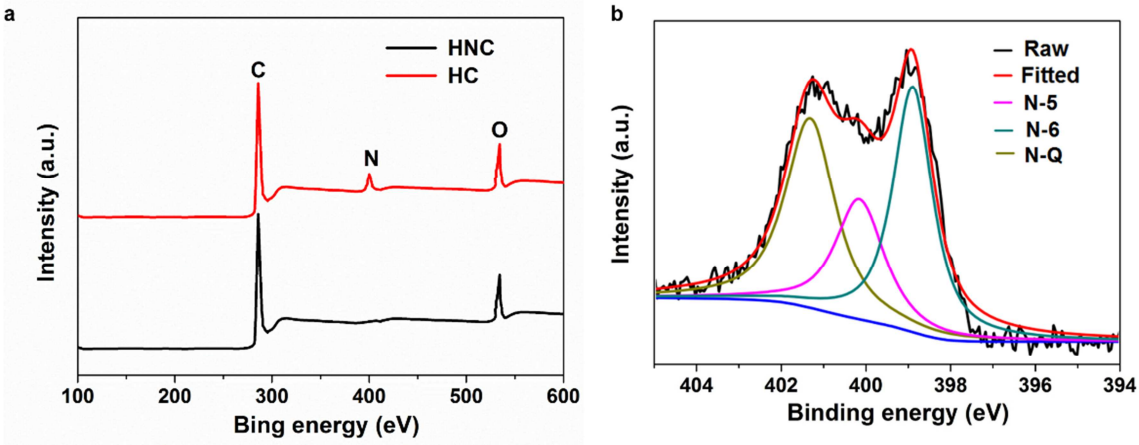

Figure 3. *XPS spectra of the hard carbon (a) survey and (b) N1s.*

The morphologies of the HNC and HC were characterized by scanning electron microscopy (SEM). All the hard carbon materials display similar morphology of lamellar structure with rough structure, which may be due to the hydrolyze and condensation of polysaccharides (Figure 2a and b). The detailed structure of samples was further investigated by high resolution transmission electron microscopy (HPTEM). The lattice spacing of the (002) crystal planes ware estimated to be 0.387 nm from the HRTEM of HNC (Figure 2c), which bigger than HC of 0.381 nm (Figure 2d), indicating N-doped can enhance the disorder of hard carbon.

The existence of nitrogen in the HNC was demonstrated by XPS. Figure 3a shows the HNC survey spectrum with three main peaks 284.6, 399.6 and 532.6 eV corresponded to the C1s, N1s and O1s, respectively [43, 45]. The relative mass percentage of C, N, and O is 77.18%, 8.68%, and 14.14%, respectively, calculated using the corresponding peak areas. The HC survey spectrum has only two main peaks of C1s and O1s. It is obvious that the nitrogen comes from the melamine with the nitrogen content as high as 66.7%. The melamine is a kind of ideal raw material for the produce of nitrogen doped caron and has been widely used. Figure 3b gives the N1s spectrum, which can be divided into three peaks centering at 398.7, 399.5 and 401.2 eV. More specific, the binding energy at 398.7 eV represents the existence of pyridinic nitrogen (N-6), 399.5 eV corresponding to pyrrolic nitrogen (N-5), while 401.2 eV assignable to graphitic nitrogen (N-Q). It can be seen that the pyridinic and graphitic N is the most nitrogen type in the HNC. The high content of pyridinic and graphitic N could facilitate the transfer of sodium ion and electrons [41, 45], which is beneficial to improve the rate capability of the anode materials.

The electrochemical performance of the HNC and HC were evaluated by galvanostatic discharge–charge test and cyclic voltammetry (CV) in the voltage range of 0.01–3.0 V versus Na/Na^+. Figure 4a and b show the initial three charge–discharge cycles curves of HNC and HC at the current density of 50 mAh g^{-1}, respectively. In the first cycle process, the discharge capacity of HNC and HC are as high as 589.8 and 603.2 mAh g^{-1}, respectively, while the charge capacity of HNC and HC are only 307.2 and 306.2 mAh g^{-1}. The large irreversible loss in the first discharge/charge process is a common phenomenon for the amorous carbon using as the anode materials for SIB and LIB [42, 46, 50], which reflected in discharge cures is the board plateau around 1 V. It is accepted that the irreversible loss is due to the formation of a solid electrolyte interface (SEI) layer and other side reactions on the surface of electrode materials [27, 39]. Notable, the discharge/charge curves of HNC are steeper than that of HC by contrast with the Figure 4a and b. In other words, more sodium ions are stored at high potential in HNC, indicating the presence of more extensive active sodium storage sites of HNC. The increased mesopores and micro pores of HNC should be the reason for the phenomenon [45, 46, 50].

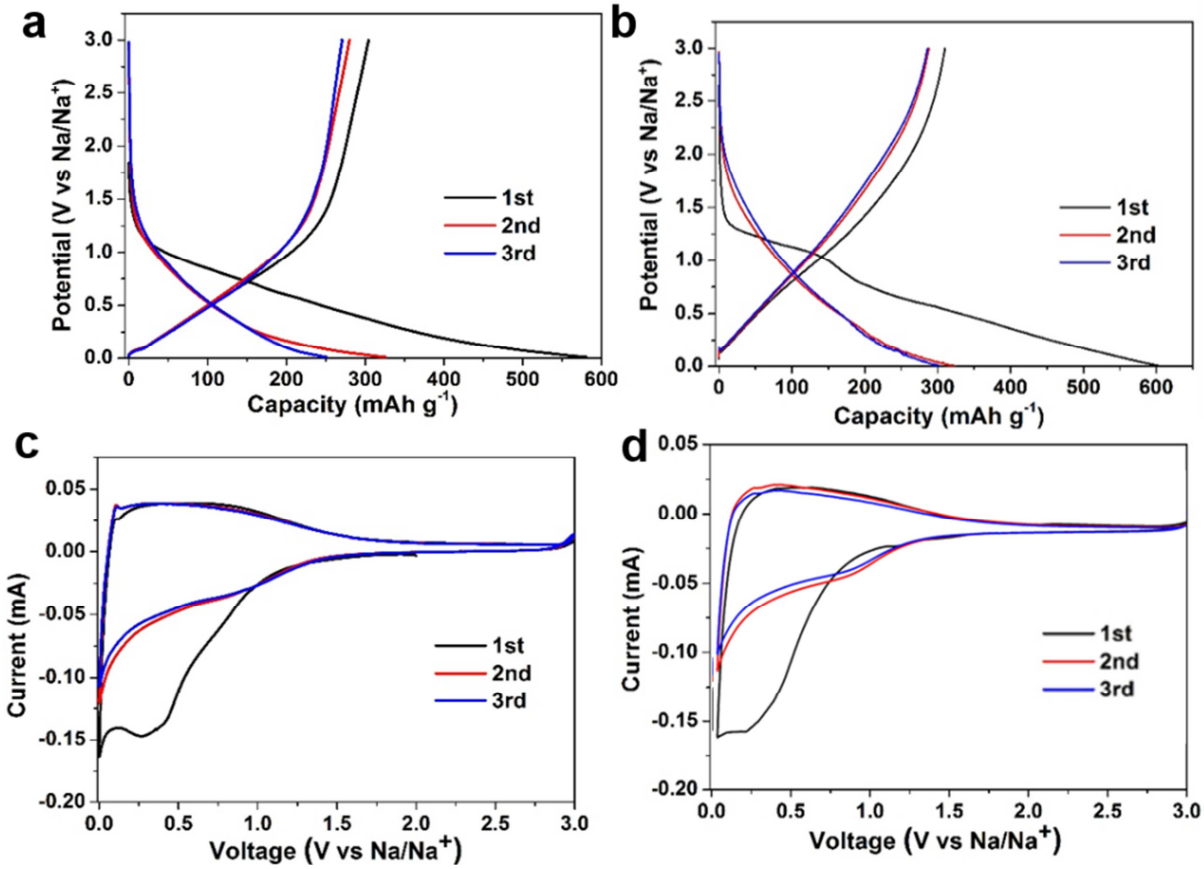

Figure 4. *Cyclic voltammetry (CV) curves of the HNC (a) and HC (b) at a scan rate of 0.1 mV s^{-1}; first three discharge/charge profiles of HNC (c) and HC (d) at a current density of 50 mA g^{-1}.*

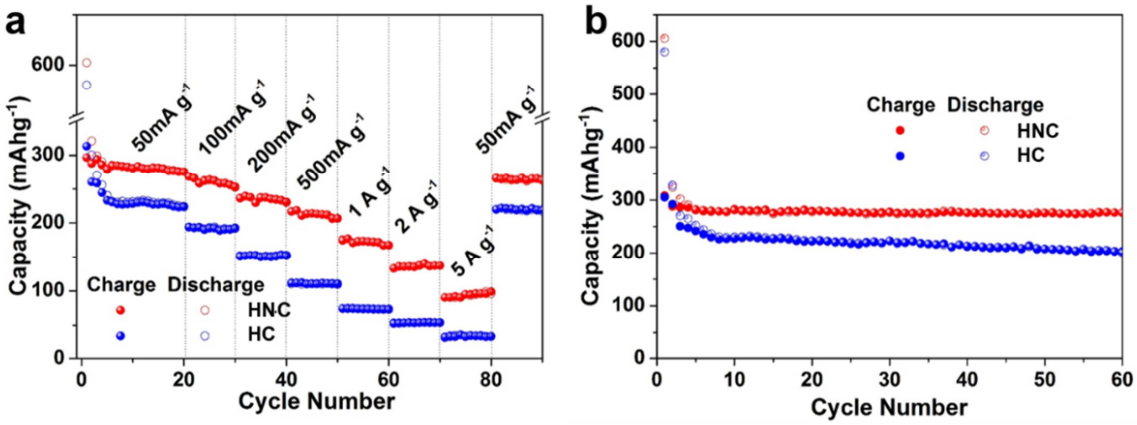

Figure 5. *Electrochemical performance of samples: (a) capacity over cycling at different rates; (b) cyclability at 50 mA g^{-1}.*

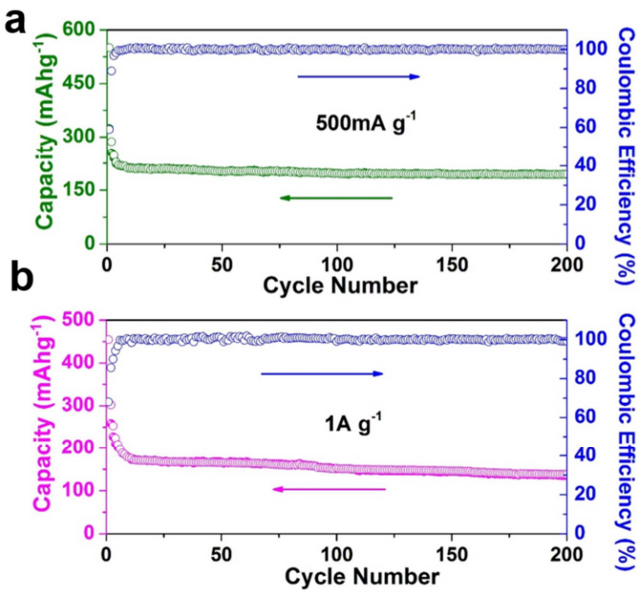

Figure 6. *Cycling property of HNC at 500 and 1000 mA g^{-1}.*

The CV date agrees well with the galvanostatic results. Figure 4c demonstrates the first three CV cycle curves of HNC. It is clear that there is a board peak started from 1.5 to 0 V in the first cathodic scan, which can be attributed to the combined effectiveness of the reaction between the sodium ion and the surface functional group, the formation of SEI film, and the insertion of sodium ion into the carbon [41, 45]. In the following cathodic scans, the board peak is divided into two obvious peaks, one at 0.75 V which is due to the reaction between the sodium ion and the surface functional group is partially reversible [45], and another at 0 V corresponding to insertion of sodium ion into the carbon. In the all anodic processes, one board peak between 0 and 1.75 V is recorded, which could be attributed to the sodium ion extraction from carbonaceous materials. Similar results of HC have been obtained shown in the Figure 4d

Figure 5a provides rate capability of HNC and HC at different current densities from 50 to 5000 mA g^{-1}. Obviously, the HNC obviously exhibits more excellent rate capacity than the HC. It exhibits the clear specific capacity gap between the HNC and HC with a continuously varying rate. The HNC shows a high reversible capacity of 296.3, 261.7 239.6 and 208.4 mAh g^{-1} at continuous change of current densities of 50, 100, 200 and 500 mA g^{-1} respectively. When the current rate increases to 1000, 2000 and 5000 mA g^{-1}, the HNC displays a higher capacity of 168.3, 121.9 and 92.7 mAh g^{-1}, and it can return back to a discharge capacity of 254.7 mAh g^{-1} at 50 mA g^{-1}.

Besides outstanding rate capacity, the cycle stability of the electrode material is an important issue for industrial applications. The cycling performance of HNC and HC were investigated at 50 mA g^{-1} for 50 cycles (Figure 5b). It can be seen that the HNC shows excellent cycle performance compared to the HC. The capacity of HNC has a slight decrease from the first cycle to the third cycle, while the capacity almost no change after three cycles. After 50 cycles, the capacity of HNC is still as high as 276 mAh g^{-1}.

Aiming at the potential applications in some special equipment, such as medical devices and lighting equipment, which require long cycle life and high power density in charge/discharge process, we also investigate the HNC at higher rate while charging/discharging as presented in Figure 6. As observed, the HNC exhibits a reversible capacity of 204.7 mAh g^{-1} (the tenth) at 500 mA g^{-1} and 190.6 mAh g^{-1} is still maintained after 200 cycles, corresponding to a capacity loss of 0.04% per cycle. Even at 1000 mA g^{-1}, a high reversible capacity of 171.6 mAh g^{-1} (the tenth) is almost the same with the capacity of HNC. After 200 cycles, the capacity decreases to 147.3 mAh g^{-1} with a capacity fading of only 0.07% per cycle. At the same time, the average coulombic efficiency of all close to 99.5%, indicating its good reversibility in the overall battery test. The outstanding performance of HNC is related to the synergetic effect of lamellar structure and high content of nitrogen. The large amount of pores is in favor of improving the area of electrode/electrolyte interface and shorting the transport length of the sodium ions. The high content of nitrogen could improve the electronic conductivity of carbon material which could facilitate the diffusion of electron. In addition, the N-doped could create a lot of defect sites, which makes for the diffusion of sodium ion in the solid phase of carbon material [33, 35]. All of them are beneficial to enhance performance of hard carbon.

To better understand the outstanding electrochemical performance of the HNC, the electrochemical impedance

spectroscopy (EIS) were measured for the charged cells of HNC and HC after 200 cycles as shown in Figure 7. It is obvious that there are two distinct parts in the Nyquist plots, depressed semicircles in the high frequency region and inclined line in the low frequency region. The semicircles at high can be assigned to the charge transfer resistance [48, 49]. The Nyquist plots show that the diameter of the semicircle of the HC is larger than that of HNC which indicates that the charge transfer resistance of the HC is higher than that of the HNC. The large charge transfer resistance of the HC may be due to the destruction of electrode structure during the charge and discharge. Moreover, the inclined line usually related with the Na-ion diffusion or so-called Warburg diffusion in the carbon electrode [48]. The sodium ion diffusion coefficient could be calculated from the low frequency plots according to the following equation [51]:

$$D = R^2T^2 / 2A^2N^4F^4C^2\sigma^2 \quad (1)$$

where R is the gas constant, T is the absolute temperature, A is the surface area of the anode, n is the number of electrons, F is the Faraday constant, C is the concentration of sodium ion. All the above parameter is the same for HNC and HC. σ is the Warburg impedance coefficient which is relative with Z_{re}.

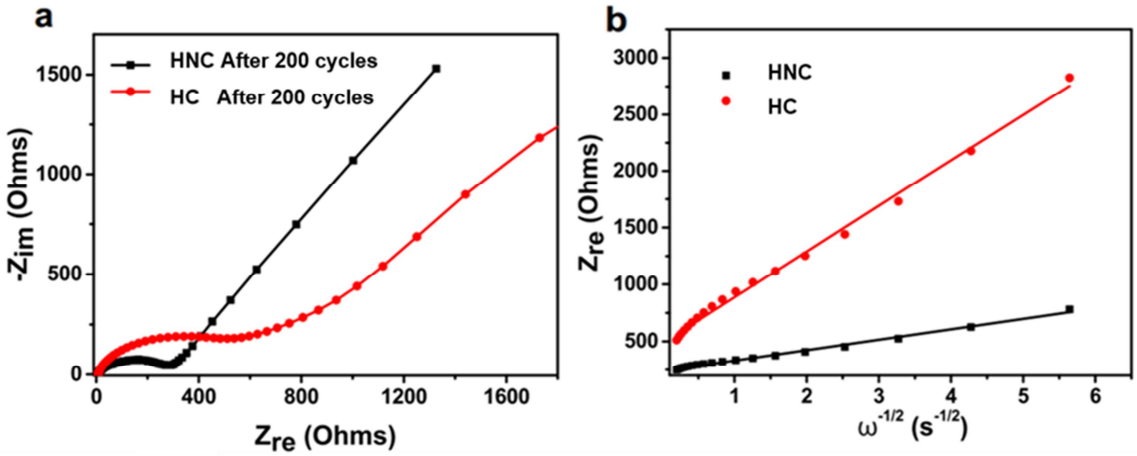

Figure 7. *(a) Nyquist plots and (b) graph of Zre plotted against$\sigma^{-1/2}$ at low frequency region of the HNC and HC after 200 cycles.*

$$Z_{re} = R + \sigma\omega^{-1/2} \quad (2)$$

Figure 7b shows the relationship between Z re and square root of frequency ($\sigma^{-1/2}$) in the low frequency region. It is observed that the r is 92 Ω cm^2 $s^{-1/2}$ for the HNC, which is lower than that off the HC (480 Ω cm^2 $s^{-1/2}$). We can further compare the sodium ion diffusion coefficient of both samples using the Eq.(1). The sodium ion diffusion coefficient of HNC is 28 times faster than that of HC. The faster sodium ion diffusion kinetic of the HNC than that of the HC can be attributed to the larger contact area of electrode/electrolyte interface and shorter transport length of the sodium ions in solid phase. It is apparent that the low charge transfer resistance and faster sodium ion diffusion kinetic would lead to the super electrochemical performance.

4. Conclusion

In this study, HNC were successfully synthesized by a simple hydrothermal reaction of cirsium setosum and subsequent thermal treatment with melamine, and used as anode materials for SIBs. The results show that HNC exhibit high capacity, excellent rate performance, long term cycling stability and ultra-fast charging/discharging ability than HC, mainly due to their stable spherical structure, large interface spacing and N-doped. A maximum capacity of 296.3 mA h g^{-1} at a current density of 50 mA g^{-1}. Even at a high current density of 500 m A g^{-1}, a capacity of 204.7 mA h g^{-1} is maintained after 200 cycles without obvious decay. The results suggest that HNC should be an attractive candidate for anodes of SIBs. nitrogen doped carbon has been successfully prepared via template-assisted method.

Acknowledgements

This work was supported by Support from the National key R&D Program of China (No. 2017YFB0308300), National Natural Science Foundation of China (No. 51472152), Natural Science Foundation of Shaanxi Province (No. 2015JM5251), Innovation Team Assistance Foundation of Shaanxi Province (No. 2013KCT-06) and the graduate Innovation Foundation of Shaanxi University of Science and Technology.

References

[1] M. Armand, J. M. Tarascon, Building better batteries, Nature 451 (2008) 652-657.

[2] J. B. Goodenough, K. S. Park, The Li-Ion Rechargeable Battery: A Perspective. J. Am. Chem. Soc. 135 (2013) 1167-1176.

[3] H. Li, D. Yu, H. Ha, et al., An All-Stretchable-Component Sodium-Ion Full Battery. Adv. Mater. 29 (2017).

[4] I. Kovalenko, B. Zdyrko, A. Magasinski, B. Hertzberg, et al., A major constituent of brown algae for use in high-capacity Li-ion batteries, Science 334 (2011) 75–79.

[5] J. W. Xu, Y. F. Wang, Z. H. Li, et al., Preparation and electrochemical properties of carbon-doped TiO_2 nanotubes as an anode material for lithium ion batteries, J. Power Sources 175 (2008) 903–908.

[6] Y. Sun, N. Liu, Y. Cui, Promises and challenges of nanomaterials for lithium-based rechargeable batteries. Nature Energy 1 (2016) 16071.

[7] H. G. Wang, W. Li, D. P. Liu, et al., Flexible Electrodes for Sodium-Ion Batteries: Recent Progress and Perspectives. Adv. Mater. 29 (2017).

[8] M. Q. Zhao, C. E. Ren, Z. Ling, et al., Flexible MXene/Carbon Nanotube Composite Paper with High Volumetric Capacitance. Adv. Mater. 27 (2014) 339-345.

[9] M. C. Lin, M. Gong, B. G. Lu, et al., An ultrafast rechargeable aluminium-ion battery, Nature 520 (2016) 324–328.

[10] Y. Sun, J. Tang, K. Zhang, et al., Comparison of reduction products from graphite oxide and graphene oxide for anode applications in lithium-ion batteries and sodium-ion batteries. Nanoscale 9 (2017) 2585.

[11] S. Y. Hong, Y. Kim, Y. Park, et al., ChemInform Abstract: Charge Carriers in Rechargeable Batteries: Na Ions vs. Li Ions. Cheminform 6 (2013) 2067-2081.

[12] L. David, R. Bhandavat, G. Singh, MoS_2/graphene composite paper for sodium-ion battery electrodes. Acs Nano 8 (2014) 1759-1770.

[13] Y. Liu, Y. Qiao, W. Zhang, et al., Nanostructured alkali cation incorporated δ-MnO 2 cathode materials for aqueous sodium-ion batteries. J. Mater. Chem. A 3 (2015) 7780-7785.

[14] X. Song, X. Li, Z. Bai, et al., Morphology-dependent performance of nanostructured Ni 3 S 2 /Ni anode electrodes for high performance sodium ion batteries. Nano Energy 26 (2016) 533-540.

[15] S. Wang, L. Xia, L. Yu, et al., Sodium Ion Batteries: Free-Standing Nitrogen‐Doped Carbon Nanofiber Films: Integrated Electrodes for Sodium-Ion Batteries with Ultralong Cycle Life and Superior Rate Capability. Adv. Energy Mater 6 (2016) n/a-n/a.

[16] D. Yan, C. Y. Yu, Y. Bai, et al., Sn-doped TiO_2 nanotubes as superior anode materials for sodium ion batteries, Chem. Commun. 51 (2015) 8261–8264.

[17] K. F. Mak, J. Shan, Photonics and optoelectronics of 2D semiconductor transition metal dichalcogenides. Nature Photonics 10 (2016) 216-226.

[18] Y. Cai, H. Yang, J. Zhou, et al., Nitrogen doped hollow MoS 2 /C nanospheres as anode for long-life sodium-ion batteries. Chem. Eng. J. 327 (2017) 522-529.

[19] M. M. Doeff, Y. Ma, S. J. Visco, et al., Electrochemical insertion of sodium into carbon, J. Electrochem. Soc. 140 (1993) 169-175.

[20] R. Alcantara, J. M. J. Mateos, J. L. Tirado, Negative electrodes for lithium and sodium-ion batteries obtained by heat-treatment of petroleum cokes below 1000°C, J. Electrochem. Soc. 149 (2002) 201-205.

[21] D. Stevens, J. Dahn, High capacity anode materials for rechargeable sodium-ion batteries, J. Electrochem. Soc. 147 (2000) 1271-1273.

[22] R. Alcantara, J. M. J. Mateos, et al., Carbon black: a promising electrode material for sodium-ion batteries, Electrochem. Commun. 3 (2001) 639–642.

[23] K. Chayambuka, G. Mulder, D. L. Danilov, et al., Sodium-Ion Battery Materials and Electrochemical Properties Reviewed. Advanced Energy Materials (2018) 1800079.

[24] Y. Xiong, J. Qian, Y. Cao, et al., Graphene-supported TiO_2 nanospheres as a high-capacity and long-cycle life anode for sodium ion batteries. J. Mater. Chem. A 4 (2016).

[25] Z. Zhu, F. Cheng, Z. Hu, et al., Highly stable and ultrafast electrode reaction of graphite for sodium ion batteries. J. Power Sources 293 (2015) 626-634.

[26] P. Thomas, D. Billaud, Sodium electrochemical insertion mechanisms in various carbon fibres, Electrochim. Acta 46 (2001) 3359-3366.

[27] R. Alcantara, P. Lavela, G. F. Ortiz, et al., Carbon microspheres obtained from resorcinol-formaldehyde as high-capacity electrodes for sodium-ion batteries, Electrochem. Solid State Lett. 8 (2005) 222–225.

[28] S. Komaba, W. Murata, T. Ishikawa, et al., Electrochemical Na insertion and solid electrolyte interphase for hard-carbon electrodes and application to Na-Ion batteries, Adv. Funct. Mater. 21 (2011) 3859–3867.

[29] Y. L. Cao, L. F. Xiao, M. L. Sushko, et al., Sodium ion insertion in hollow carbon nanowires for battery applications, Nano Lett. 12 (2012) 3783–3787.

[30] T. Q. Chen, L. K. Pan, T. Lu, et al., Fast synthesis of carbon microspheres via a microwave-assisted reaction for sodium ion batteries, J. Mater. Chem. A. 2 (2017) 1263–1267.

[31] T. Q. Chen, Y. Liu, L. K. Pan, et al., Electrospun carbon nanofibers as anode materials for sodium ion batteries with excellent cycle performance, J. Mater. Chem. A 2 (2016) 4117–4421.

[32] L. J. Fu, K. Tang, K. P. Song, et al., Nitrogen doped porous carbon fibres as anode materials for sodium ion batteries with excellent rate performance, Nanoscale 6 (2016) 1384–1389.

[33] Z. H. Wang, L. Qie, L. X. Yuan, et al., Functionalized N-doped interconnected carbon nanofibers as an anode material for sodium-ion storage with excellent performance, Carbon 55 (2015) 328–334.

[34] H. G. Wang, Z. Wu, F. L. Meng, et al., Nitrogen-doped porous carbon nanosheets as low-cost, high-performance anode material for sodium-ion batteries, ChemSusChem 6 (2015) 56–60.

[35] J. T. Xu, M. Wang, N. P. Wickramaratne, et al., High-performance sodium ion batteries based on a 3D anode from nitrogen-doped graphene foams, Adv. Mater. 27 (2015) 2042–2048.

[36] K. Tang, L. Fu, R. J. White, et al., Hollow carbon nanospheres with superior rate capability for sodium-based batteries, Adv. Energy Mater. 2 (2012) 873–877.

[37] C. H. Choi, S. H. Park, S. I. Woo, Binary and ternary doping of nitrogen, boron, and phosphorus into carbon for enhancing electrochemical oxygen reduction activity, ACS Nano. 6 (2012) 7084–7091.

[38] M. M. Doeff, Y. Hu, F. M. Larnon, et al., Effect of surface carbon structure on the electrochemical performance of $LiFePO_4$, Electrochem. Solid-State Lett. 6 (2003) A207–A209.

[39] Y. Y. Shao, J. Xiao, W. Wang, et al., Surface-driven sodium ion energy storage in nanocellular carbon foams, Nano Lett. 13 (2013) 3909–3914.

[40] Z. R. Ismagilov, A. E. Shalagina, O. Y. Podyacheva, et al., Structure and electrical conductivity of nitrogen-doped carbon nanofibers, Carbon 47 (2009) 1922–1929.

[41] Z. Zhong, G. I. Lee, C. B. Mo, et al., Tailored field-emission property of patterned carbon nitride nanotubes by a selective doping of substitutional N (sN) and pyridine-like N (pN) atoms, Chem. Mater. 19 (2007) 2918–2920.

[42] Y. Wu, S. Fang, Y. Jiang, Effects of nitrogen on the carbon anode of a lithium secondary battery, Solid State Ionics 120 (1999) 117–123.

[43] T. Sharifi, G. Z. Hu, X. Jia, et al., Formation of active sites for oxygen reduction reactions by transformation of nitrogen functionalities in nitrogen-doped carbon nanotubes, ACS Nano 6 (2012) 8904–8912.

[44] W. Shen, C. Wang, Q. J. Xu, et al., Nitrogen-doping-induced defects of a carbon coating layer facilitate Na-storage in electrode materials, Adv. Energy Mater. 5 (2015) 1400982

[45] S. Y. Wang, X. S. Zhao, T. Cochell, et al., Nitrogen-doped carbon nanotube/graphite felts as advanced electrode materials for vanadium redox flow batteries, J. Phys. Chem. Lett. 3 (2012) 2164–2167.

[46] B. S. Lee, S. B. Son, K. M. Park, et al., Anodic properties of hollow carbon nanofibers for Li-ion battery, J. Power Sources 199 (2012) 53–60.

[47] E. Buiel, A. E. George, J. R. Dahn, On the reduction of lithium insertion capacity in hard-carbon anode materials with increasing heat-treatment temperature, J. Electrochem. Soc. 145 (1998) 2252–2257.

[48] E. J. Yoo, J. Kim, E. Hosono, et al., Large reversible Li storage of graphene nanosheet families for use in rechargeable lithium ion batteries, Nano Lett. 8 (2008) 2277–2282.

[49] D. A. Stevens, J. R. Dahn, An in situ small-angle X-ray scattering study of sodium insertion into a nanoporous carbon anode material within an operating electrochemical cell, J. Electrochem. Soc. 147 (2000) 4428–4431.

[50] K. Chang, W. X. Chen, L-cysteine-assisted synthesis of layered MoS_2 /grapheme composites with excellent electrochemical performances for lithium ion batteries, ACS. Nano. 5 (2011) 4720–4728.

[51] H. M. Xie, R. S. Wang, J. R. Ying, et al., Optimized $LiFePO_4$-polyacene cathode material for lithium-ion batteries, Adv. Mater. 18 (2006) 2609–2613.